

Observing cosmic string loops with gravitational lensing surveys

Katherine J. Mack^{1,2,3*}

¹*Department of Astrophysical Sciences, Princeton University*

Daniel H. Wesley^{2†}

²*Department of Applied Mathematics and Theoretical Physics, Cambridge University*

Lindsay J. King^{3‡}

³*Institute of Astronomy, Cambridge University*

We show that the existence of cosmic strings can be strongly constrained by the next generation of gravitational lensing surveys at radio frequencies. We focus on cosmic string loops, which simulations suggest would be far more numerous than long (horizon-sized) strings. Using simple models of the loop population and minimal assumptions about the lensing cross section per loop, we estimate the optical depth to lensing and show that extant radio surveys such as CLASS have already ruled out a portion of the cosmic string model parameter space. Future radio interferometers, such as LOFAR and especially SKA, may constrain $G\mu/c^2 < 10^{-9}$ in some regions of parameter space, outperforming current constraints from pulsar timing and the CMB by up to two orders of magnitude. This method relies on direct detections of cosmic strings, and so is less sensitive to the theoretical uncertainties in string network evolution that weaken other constraints.

*Electronic address: mack@astro.princeton.edu

†Electronic address: D.H.Wesley@damtp.cam.ac.uk

‡Electronic address: ljk@ast.cam.ac.uk

I. INTRODUCTION

Cosmic strings are linear, relativistic objects whose existence is predicted by a number of extensions to the Standard Model of particle physics [1, 2, 3]. When first proposed, they were intensely studied as a possible mechanism for cosmological structure formation. This scenario is now known to be inconsistent with a variety of cosmological constraints [4, 5, 6, 7, 8, 9, 10, 11, 12, 13, 14], but recently cosmic strings have attracted renewed interest thanks to the postulation of new types and new production mechanisms. The current focus has shifted from their role in structure formation to the prospects for detecting them if they are present [7, 8, 15, 16, 17, 18].

Here we describe a method to detect cosmic string loops using strong gravitational lensing of compact radio sources. We propose searching for loops because simulations suggest there could be $> 10^5$ per horizon volume in contrast to only ~ 40 long (horizon-sized) strings [2, 3]. Compact radio sources (hereafter CRSs) are an ideal source population since their point-like nature on angular scales < 100 mas makes lensed images easy to identify. Furthermore, numerous CRSs have been observed by radio surveys such as the Cosmic Lens All-Sky Survey (CLASS) and are expected to be observed by proposed surveys such as the Low Frequency Array (LOFAR) and the Square Kilometer Array (SKA). In this paper, we estimate the expected number of loop lensing events for these three surveys as a function of cosmic string model parameters, and find that for significant regions of parameter space our method can outperform existing constraints.

An important feature of our method is that it would constitute a *direct detection* rather than an inference based on assumed or simulated properties of a cosmic string network. By contrast, the pulsar timing constraint (the most stringent constraint to date) requires knowledge of the rate of emission of gravitational waves by oscillating strings and of properties of the loop population. As we will discuss below, the signatures of lensing by a string loop are distinctively different from those of lensing by a galaxy (which will generally have a similar image separation in the arcsecond regime). Follow-up observations should be able to quickly determine if putative lensing events are due to cosmic strings or to more conventional astronomical objects. In past gravitational lensing surveys, all lensing events have been associated with conventional lensing objects such as galaxies or clusters after follow-up observations. We rely on the reasonable expectation that sufficient follow-up is always

performed; a constraint will be obtained if all lensing events are accounted for by standard lenses and are therefore not cosmic string lensing candidates. If after deep imaging a conventional lensing object was not observed, the lens would be classified as “dark” and modelling of the gravitational potential would be required to rule it out as a cosmic string. As of yet, no confirmed dark lenses have been found.

Either a detection of, or a constraint on, cosmic strings would be important for understanding physics beyond the Standard Model. Cosmic strings can be accommodated in many superstring models, and indeed are predicted to be present in brane inflation scenarios [19, 20, 21, 22, 23, 24, 25]. The wide range of string tensions and the novel features of cosmic strings predicted by these models present a challenge to observation. By tightening constraints on cosmic strings, we are indirectly testing these models and learning about physics at high energies and early times in the history of the universe.

This paper is organized as follows. In Section II we describe our assumptions about the properties of the loop lenses, discuss our population models, and describe the telescopes and surveys proposed for the observation. We present the results of the calculation in Section III, giving the expected number of lensing events as a function of parameters of the string model and comparing the constraint obtained to those presently available. We conclude in Section IV and discuss areas in which future work is needed.

II. METHODOLOGY

We now describe our calculation of the expected number of observable string loop lensing events. We do this by combining estimates of the area of sky that can be strongly lensed by loops, the resolution and dynamic range of the instrument employed, and the source population abundance, which is a function of instrument and survey parameters as well as of the intrinsic abundance.

To estimate of the fraction of the sky that is strongly lensed by the loop population we must confront the significant theoretical uncertainties in both (i) the lensing characteristics of individual loops, and (ii) the distribution of lengths in the loop population as a function of redshift. To deal with (i) we take a statistical approach: we assume that each loop can form multiple images of all sources in a patch of sky of angular area $\pi\theta_E^2$, with image separations of at least θ_E , where θ_E is the Einstein radius of a Schwarzschild lens with the same mass

as the loop.

Realistic loops will be of highly irregular shape and can produce complicated lensing patterns, which have been considered in detail elsewhere [26, 27, 28, 29]. However, we expect that the lensing cross section, when averaged over a population of loops of fixed mass, will be close to the characteristic area set by the Schwarzschild lens. We justify our approximation in Section II A by comparing it to the exact results in cases where loop lensing can be studied analytically. To model the loop population as required by (ii), we use two simple models, which we discuss in Section II B, with the string tension μ a free parameter in both. The first is a powerlaw distribution of loop lengths, defined by a spectral index γ , the loop density parameter Ω_{loop} , and a cutoff length L_* . The second model is derived from the one-scale model, a semi-analytic model of string networks widely discussed in the literature. This model has a number of parameters, but in addition to μ we consider only α (which sets the size of newly created loops) to be free.

We then turn to the source population and instruments. In Section II C we argue that compact radio sources make ideal source candidates for investigating lensing by loops, and we discuss some of their features. In Section II D, we describe both extant surveys (CLASS) and proposed instruments (LOFAR and SKA) that will observe these objects. Our discussion focuses on the parameters of these surveys that are most relevant to a prediction of the number of string loop lensing events expected in each survey, namely the angular resolution and sensitivity. The angular resolution sets the minimum separation of images which may be detected, and hence the minimum string tension of observable loops. The sensitivity of the instrument influences the number of potential targets for lensing, since a more sensitive instrument will pick up fainter or more distant sources.

A. Loops as lenses

We rely on the approximation, justified below, that a loop of mass M_{loop} produces multiple images of background sources situated in a patch of sky of area $\pi\theta_E^2$, and that the images are separated by at least θ_E , where θ_E is the Einstein radius of a Schwarzschild lens having the same mass as the loop. The Einstein radius for a loop of mass M_{loop} is given by

$$\theta_E = \sqrt{\frac{4GM_{loop}}{c^2} \frac{D_{LS}}{D_L D_S}} \quad (1)$$

where D_L , D_S and D_{LS} are the angular diameter distances between the observer and lens, observer and source, and lens and source, respectively [30].

To justify this approximation we compare it to the sky area lensed by a circular loop of radius R and angular radius $\theta_{loop} = R/D_L$ situated in a plane perpendicular to the line of sight. Light rays passing outside the loop are deflected as if by a Schwarzschild lens of the same mass as the loop, while those passing through the loop are not deflected. A pure Schwarzschild lens always produces two images of a source at angles θ_{\pm} from the lens, given by

$$\theta_{\pm} = \frac{\theta_S \pm \sqrt{\theta_S^2 + 4\theta_E^2}}{2}, \quad (2)$$

where θ_S is the (unlensed) angular position of the source. For a loop, any images at $\theta < \theta_{loop}$ are spurious, since the corresponding light rays must have passed through the loop, and will not be observed. The unlensed source itself will be visible through the loop if $\theta_S < \theta_{loop}$.

The region of $(\theta_S, \theta_{loop})$ parameter space in which multiple images form is shown in Figure 1. While multiple images are always created by a Schwarzschild lens, the “+” and “-” images are produced with different fluxes, and if the flux ratio is too large then the pair will not be observed as a lens. Imposing a conservative flux ratio $\leq 10:1$ for our calculations means that the “-” image will only be included if $\theta_S < 1.125\theta_E$, which cuts off the multiple lensing region for the “-” image. The source and “+” image have a flux ratio that is nearly unity, which enhances the prospects for lens identification when both are present. When $\theta_{loop} \leq \theta_E$ there is always at least one pair of images separated by $\geq 2\theta_E$. For $\theta_{loop} > \theta_E$, the image separations gradually decrease from θ_E when $\theta_{loop} \sim \theta_E$, and go as θ_E^2/θ_{loop} for $\theta_{loop} \gg \theta_E$. The patch of sky for which multiple images form when $\theta_{loop} > \theta_E$ has area

$$\pi\theta_E^2 (2 - [\theta_E/\theta_{loop}]^2) \quad (3)$$

which is always greater than $\pi\theta_E^2$. One can show that the sky area (3) asymptotes to that of a long straight string as $\theta_E/\theta_{loop} \rightarrow 0$, corresponding to $R \rightarrow \infty$.

Our approximation accurately reflects the lensing cross section in the special case of a planar circular loop. However, the area lensed by a typical loop most likely exceeds this. A circular loop is the least dense arrangement of the loop’s mass, and furthermore rays passing through the loop are not lensed at all. A realistic loop will likely be “crumpled,” concentrating the mass and better approximating a Schwarzschild lens for a larger range of impact parameters. In the limit that the loop can be treated as a random walk with step

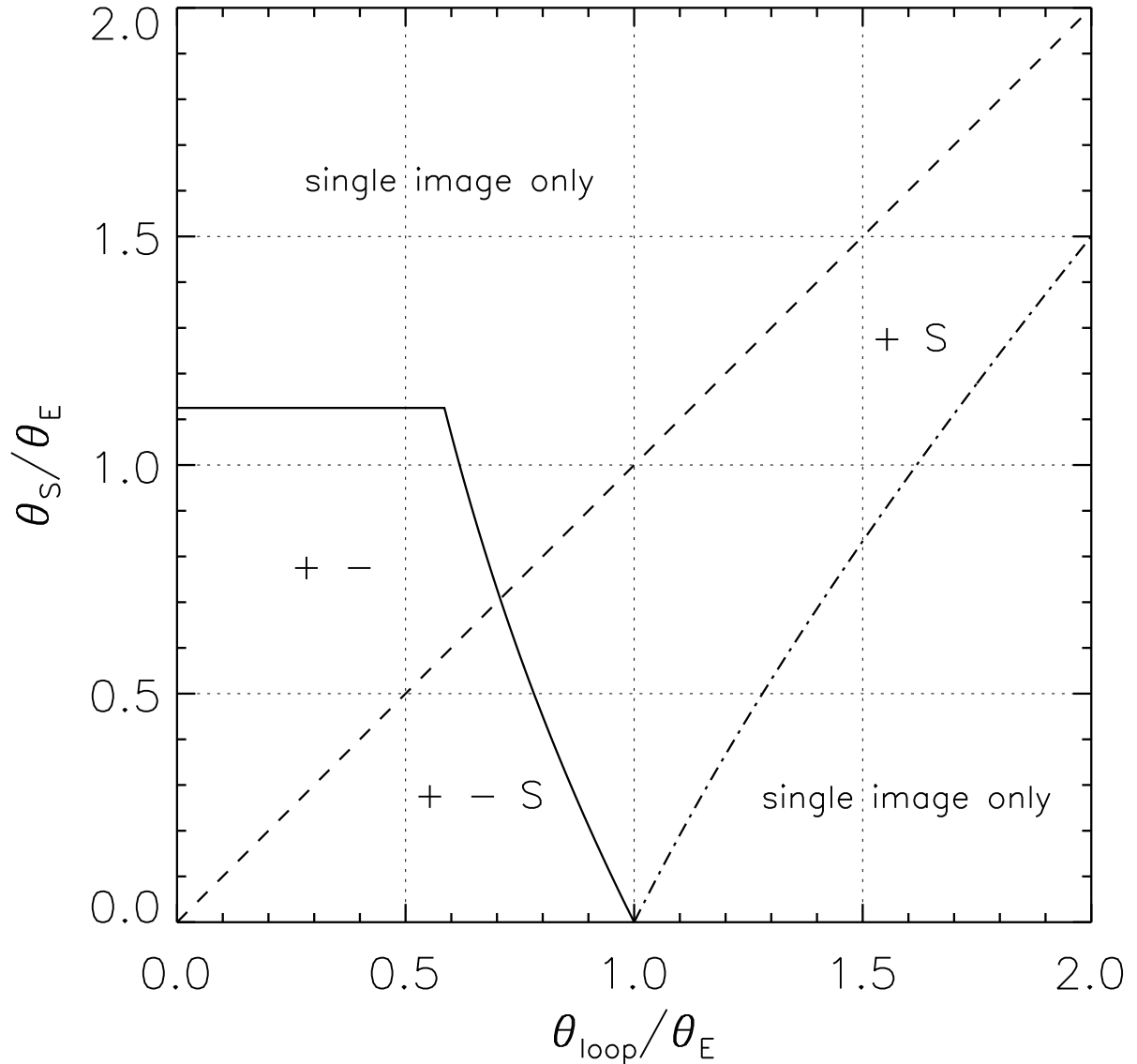


FIG. 1: Regions of the $(\theta_S, \theta_{loop})$ parameter space where multiple images are formed by a planar circular loop. Regions are labeled depending on whether the \pm Schwarzschild images are formed, or whether direct images of the source (S), are visible.

size (correlation length) l_c , then a loop of radius R , when crumpled, will fit in a sphere of radius $C\sqrt{l_c R}$, with C a constant of order unity. This reduces the angle θ_{loop} subtended by the loop by the factor $C\sqrt{l_c/R}$, which will be significant for large loops. There are other effects that may also increase the area of the lensed patch of sky, which we will discuss in Section IV.

B. Loop population models

We now describe our two models of the loop length distribution, defined by a number density per logarithmic interval in the loop length L , $N_L(L, z) = dN(z)/d \ln L$. Here N is the number of loops in a comoving volume $(c/H_0)^3$, where c is the speed of light and H_0 is today's Hubble parameter. The first model is the simplest scale-free distribution, a powerlaw in the loop length. It is not motivated by any model of string network evolution that we are aware of, but is useful for understanding how the constraint depends on basic features of the loop length spectrum and may describe other lens populations. The second model is more realistic. It uses the loop length spectrum derived from the one-scale model (OSM) of cosmic string network evolution, a semi-analytic model that fits well to full-scale simulations.

1. Powerlaw loop spectrum

For the powerlaw spectrum, assuming a constant comoving density of loops, we have

$$N_L(L, z) = \Omega_{loop,0} \frac{\rho_{crit,0} |\gamma|}{\mu L_*} \left(\frac{c}{H_0} \right)^3 \left(\frac{L}{L_*} \right)^{\gamma-1}, \quad (4)$$

where $\Omega_{loop,0}$ is the present mass parameter in loops, and $\rho_{crit,0}$ is today's critical density. L_* is a loop length cutoff, so we include only $L < L_*$ when $\gamma > 0$, or $L > L_*$ when $\gamma < 0$. If we instead assume a constant number of loops per particle horizon volume we obtain

$$N_L(L, z) = \Omega_{loop} \frac{\rho_{crit,0} |\gamma|}{\mu L_*} \left(\frac{c}{H_0} \right)^3 \left(\frac{L}{L_*} \right)^{\gamma-1} \left[\frac{H(z)}{H_0} \right]^3. \quad (5)$$

To better compare with the one-scale model (discussed in the following section) we will use this assumption (equation 5) in all our calculations with the powerlaw model henceforth.

For the present work we will only consider $\gamma < 0$, as suggested by string network simulations [31, 32]. The effective lower cut-off on the powerlaw loop spectrum then comes from the smaller of L_* and the resolution limit. In practice, Ω_{loop} and L_* are degenerate in the sky fraction calculation, so for this work we fix $L_* = 1$ kpc and vary Ω_{loop} only. The upper limit on the loop spectrum integration is chosen so that loops longer than $L_{max} = (\epsilon/(1+\epsilon))^{1/\gamma} L_*$, which account for a fraction ϵ of the total number of loops, are left out. In cases where the instrumental resolution is high enough to resolve loops all the way down to the lower cut-off L_* , defining the upper cut-off in this way results in the sky fraction being independent of γ .

2. One-scale model

The one-scale model is a simple model of string networks, supported by numerical simulations: a detailed exposition may be found in [4]. The only length scale in this model is $\ell(t)$, the radius of the particle horizon at a time t . Loops that form at time t have length $\alpha\ell(t)$, with α a constant, and subsequently shrink by emitting gravitational radiation. The rate of loop formation is found by requiring that a sufficient number of loops are formed to keep the number of long strings per particle horizon volume constant. In principle, α can be determined from numerical simulations, but as yet a clear consensus on its value has not emerged, so we take it to be a free parameter.

By assuming a matter-dominated universe one finds

$$\frac{dN}{d \ln L} = \frac{1 + \frac{\alpha/[G\mu/c^2]}{23.5}}{50.3\alpha[G\mu/c^2]} \frac{L/\ell_{H_0}}{\left(1 + \frac{L}{33.3[G\mu/c^2]\ell_{H_0}}\right)^2} \quad (6)$$

where $\ell_{H_0} = c/H_0$, and we have used the values for other one-scale model parameters in [4]. This distribution has a peak at $L_{peak} \sim 33\ell_{H_0}[G\mu/c^2]$, and the spectral index $\gamma = 0$ for $L > L_{peak}$ and $\gamma = +2$ for $L < L_{peak}$. It has an upper cutoff at $L = \alpha\ell(t) = 2\alpha\ell_{H_0}$ (during the matter era); this is the length at which loops are created. Using this spectrum, the density parameter in loops is

$$\Omega_{loop} = \left[\frac{G\mu}{c^2}\right] \frac{185}{y} \left(1 + \frac{y}{23.5}\right) \left[\ln \left(1 + \frac{y}{16.7}\right) - \left(1 + \frac{16.7}{y}\right)^{-1} \right] \quad (7)$$

where $y \equiv \alpha/(G\mu/c^2)$. These equations are derived in detail in Appendix A.

C. Compact Radio Sources

Selection of a background source population has a major impact on the efficiency and completeness of a gravitational lensing survey. For many background sources with extended emission, multiple imaging can be mistaken for the intrinsic structure of the source, or vice-versa. In order to easily determine whether or not lensing has occurred, the best strategy is to optimize the survey to observe sources that are intrinsically point-like (to prevent the misidentification of substructure) and to use instruments with resolution high enough to distinguish the images produced by a typical lensing event. With this in mind,

we consider a source population of flat spectrum compact radio sources (CRSs), which are single-component sources at ~ 100 mas resolution. These sources are numerous at high redshifts; typically $z \sim 1 - 2$ over a few magnitudes in flux density (see, e.g., [33, 35]). This enables us to probe a large cosmological volume. Compact radio sources are also ideal for the purpose of optimizing the survey resolution, as long-baseline radio interferometry routinely reaches sub-arcsecond resolution. Furthermore, radio sources may be significantly polarized, offering a further check that lensing is indeed occurring, as well as providing additional constraints on lens models.

The signatures of lensing by cosmic string loops would be quite different from those seen in lensing by galaxies. In every instance of lensing by a galaxy, the lens would be identified by its presence in follow-up optical or near-infrared observations (normal elliptical and spiral galaxies are fairly radio quiet). In addition, lens modeling would indicate whether the lens has a mass density profile compatible with a galaxy, the majority of which have near isothermal profiles on the scales relevant to strong lensing [34]. The polarization of the images would also help to differentiate between lensing by galaxies and by cosmic string loops. In galaxy lensing, any polarized emission of the source is affected by Faraday rotation as it passes through the interstellar medium of the lens galaxy, resulting in (frequency-dependent) differences in the polarization position angles of the images; this would not occur if the lens was a cosmic string loop. Using these criteria it will be straightforward to rule out lensing by a galaxy, and careful follow-up imaging and spectroscopic observations will make it possible to determine if the lens is any known astrophysical object.

D. Radio Surveys

Having described the fraction of sky that could be lensed by string loops, and having selected our source population, we now discuss some instruments and surveys that might observe loop lensing events. Key features that will serve as inputs to the estimated number of lensing events are the dynamic range, resolution, and expected source counts for each survey.

CLASS/JVAS. The Cosmic Lens All-Sky Survey (CLASS) [36, 37] and the Jodrell Bank VLA Astrometric Survey (JVAS) [38] searched for gravitationally lensed flat spectrum radio sources. Together, they targeted 16503 sources, of which 11685 have flat spectra (spectral

index flatter than 0.5 between 1.4 and 5 GHz) and flux density $\geq 30\text{mJy}$ at 5 GHz. The statistically well defined sample of 11 lens systems found includes only those with separations in excess of 0.3-arcsec and flux ratio $\leq 10:1$.

LOFAR. The Low Frequency Radio Array (LOFAR) is expected to be operational by the end of 2008, initially with a maximum baseline of 100 km, and maximum resolution of ~ 3 arcsec, which would only detect the largest separation events. Therefore, we concentrate on a proposed extension to LOFAR with a maximum baseline of 400 km [39]. Two planned surveys are relevant to lensing: one at 200 MHz over 250 deg^2 at 0.8-arcsec resolution, and the other at 120 MHz over half the sky with a resolution of 1.3 arcsec [40]. The former will include 3×10^7 sources to the $14\mu\text{Jy}$ limit and the latter 8.6×10^8 sources to $43\mu\text{Jy}$. These source counts are expected to be dominated by steep spectrum galaxies, with $\sim 5\%$ being flat-spectrum [41].

SKA. The Square Kilometre Array (SKA), planned to be fully operational by 2020, will consist of thousands of radio antennae with a collecting area exceeding thirty times that of the largest telescope ever constructed. The site and specifications have yet to be finalized; we adopt the estimates from [42]. They discuss a possible Radio All-SKA Lens survey (RASKAL) of half the sky at 1.4 GHz, with 0.01-0.02-arcsec resolution. Limiting to sources brighter than $3\mu\text{Jy}$ there would be $\sim 10^9$ radio sources, of which roughly 10% would be compact, flat-spectrum sources – the ideal target for a statistically complete lens survey. As with CLASS/JVAS, the median redshift is expected to be $z > 1$.

We summarize the properties of the surveys we consider in Table I. For Extended LOFAR, we take the higher-resolution 240 MHz survey, and for SKA we assume the optimistic end of the resolution range, 0.01 arcsec. In the table, “number of sources” refers to the number of CRSs accessible to the survey. Based on estimates in [33] of the mean redshift of CRSs, for the purpose of this study we choose a redshift of $z = 1.2$ for our source population in all surveys. The true distribution of CRSs is still incompletely understood, especially for the flux limits that can be reached by future surveys. We expect that this approximation affects our result by less than an order of magnitude.

III. RESULTS

A. Expected Lensing Events

We estimate the number of cosmic string loop lensing events one can expect to observe in past and future compact radio source gravitational lensing surveys whose properties can be found in Table I. Our main results are summarized in Figures 2 and 3.

1. Powerlaw models

For a powerlaw loop length spectrum with a negative spectral index, most loops will be small. This is a disadvantage in a lensing search because of image separation: lensing events from small loops are likely to be lost due to resolution limits. With CLASS/JVAS, we expect to see few lensing events in the survey over most of the range of plausible powerlaw indices and loop density parameters. LOFAR will have the ability to rule out a slightly larger portion of the parameter space, for $\Omega_{loop} \gtrsim 10^{-2}$ and $\gamma \gtrsim -1$. When $\gamma < 0$, the sky fraction is strongly dependent on the instrument’s ability to resolve the smallest loops; both CLASS/JVAS and LOFAR lack the resolution to be effective in this regime. With the high resolution of SKA, however, nearly all loops will be resolved for powerlaw indices $-3 < \gamma < 0$ with $L_* = 1$ kpc, and the large number of compact radio sources available will allow us to rule out to $3\text{-}\sigma$ a density parameter in loops of $\sim 10^{-7}$ if no loop lensing events are observed. The results for the powerlaw loop spectrum are presented in Figure 2. (Note that these results could easily be translated into constraints on any population of point masses with a powerlaw mass spectrum, which may include some models of primordial black holes [43].)

TABLE I: Properties of Gravitational Lensing Surveys

Survey	Resolution (arcsec)	Number of Sources (observed/expected)
CLASS/JVAS	0.3	11685
Ext. LOFAR	0.8	1.5×10^6
SKA	0.01	10^8

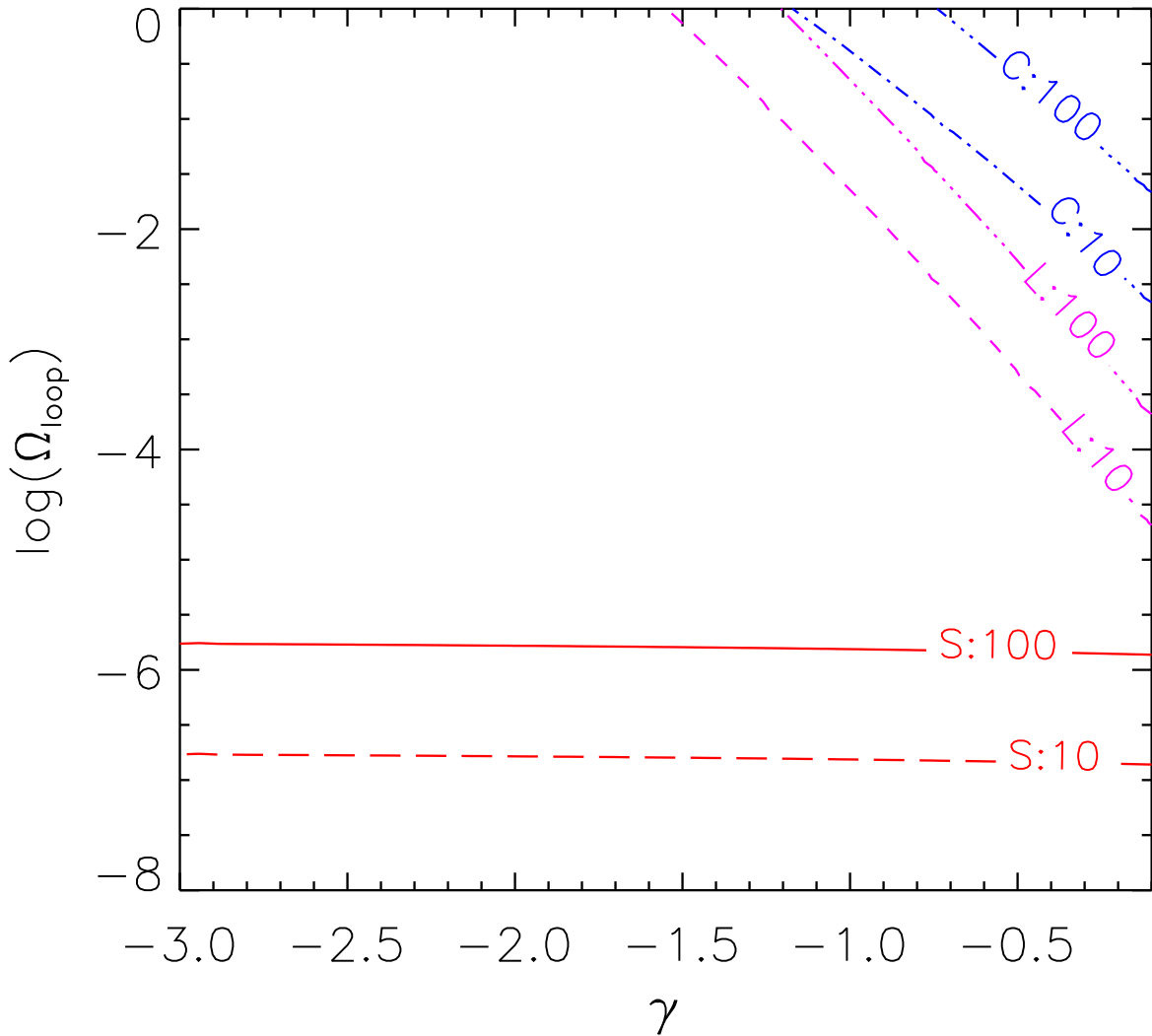


FIG. 2: Contours for 10 and 100 expected events using the powerlaw loop spectrum model for CLASS/JVAS (C), LOFAR (L) and SKA (S), for a source population at redshift $z=1.2$. The x-axis is the powerlaw index γ (see Section II B 1) and the y-axis is the density parameter in loops, Ω_{loop} . 10 expected events corresponds to a constraint at 3σ if no events are observed.

2. One-scale model.

Our results for a one-scale model spectrum of loops are presented in Figure 3 for the CLASS/JVAS, LOFAR and SKA surveys. The one-scale model spectrum has two limiting cases of interest, depending on the relationship between $G\mu/c^2$ and α .

When $\alpha \lesssim 16G\mu/c^2$, the upper cut-off in the spectrum is below the peak, and thus the

spectrum is approximately a powerlaw with spectral index +2 and is dominated by loops near the upper cut-off at $2\alpha\ell_{H_0}$. For a powerlaw spectrum as in Equation 4 with $\gamma > 0$, the mass density goes as

$$\rho \sim \left(\frac{G\mu}{c^2}\right) N_0 L_{max}^{1-\gamma} (L_{max}^\gamma - L_{min}^\gamma), \quad (8)$$

with $N_0 \sim \Omega_{loop}/([G\mu/c^2]L_{max})$. This means that the mass density $\rho \sim \Omega_{loop} \sim 1/\alpha$. Ignoring resolution effects, the sky fraction is proportional to the mass density, since $\theta_E^2 \sim M_{loop}$, so in this regime, the sky fraction is independent of $G\mu/c^2$. When α is small, the resolution of the instrument also decreases the sky fraction because the smallest image separations will be lost.

When $\alpha \gg G\mu/c^2$, the mass in loops is dominated by the region of the spectrum with a spectral index of 0. For $\gamma = 0$, $\rho \sim (G\mu/c^2)N_0 \ln(L_{max}/L_{min})$. Since the low-mass end of the spectrum gives a small contribution, one can approximate the lower cut-off as the peak position: $L_{min} \sim L_{peak} \sim G\mu/c^2$. L_{max} is the upper cut-off which goes as α . In this case, $N_0 \sim \Omega_{loop}/([G\mu/c^2] \ln \alpha/[G\mu/c^2])$. Since in the limit that $\alpha \gg G\mu/c^2$, $\Omega_{loop} \sim (G\mu/c^2) \ln \alpha/(G\mu/c^2)$, one finds that $\rho \sim (G\mu/c^2) \ln \alpha/(G\mu/c^2)$. In this regime, the sky fraction depends only very weakly on α .

If the loop spectrum follows the one-scale model, we can rule out regions of the parameter space to $3\text{-}\sigma$ even with the CLASS/JVAS survey, as seen in Figure 3. This plot also shows that a large region of parameter space can be ruled out with LOFAR or SKA. With SKA, a $3\text{-}\sigma$ constraint will be achievable down to $G\mu/c^2 \sim 10^{-9}$ for large values of α . In the next section, we discuss how loop lensing surveys can be more powerful and more direct than current methods to constrain cosmic strings with pulsar timing.

B. Comparison with other constraints

Currently, the strongest limits on cosmic strings come from constraints on the stochastic gravitational wave background obtained from the timing of millisecond pulsars [44]. In the context of the one-scale model, pulsar timing constrains a combination of $G\mu/c^2$ and α .

In Figure 3, we include the pulsar timing constraint from [45] for two different values of the density parameter in gravitational waves for comparison with the limits we can obtain with radio surveys. The limit obtainable from SKA can improve upon the pulsar timing constraint by up to two orders of magnitude in $G\mu/c^2$ in some regions of the parameter

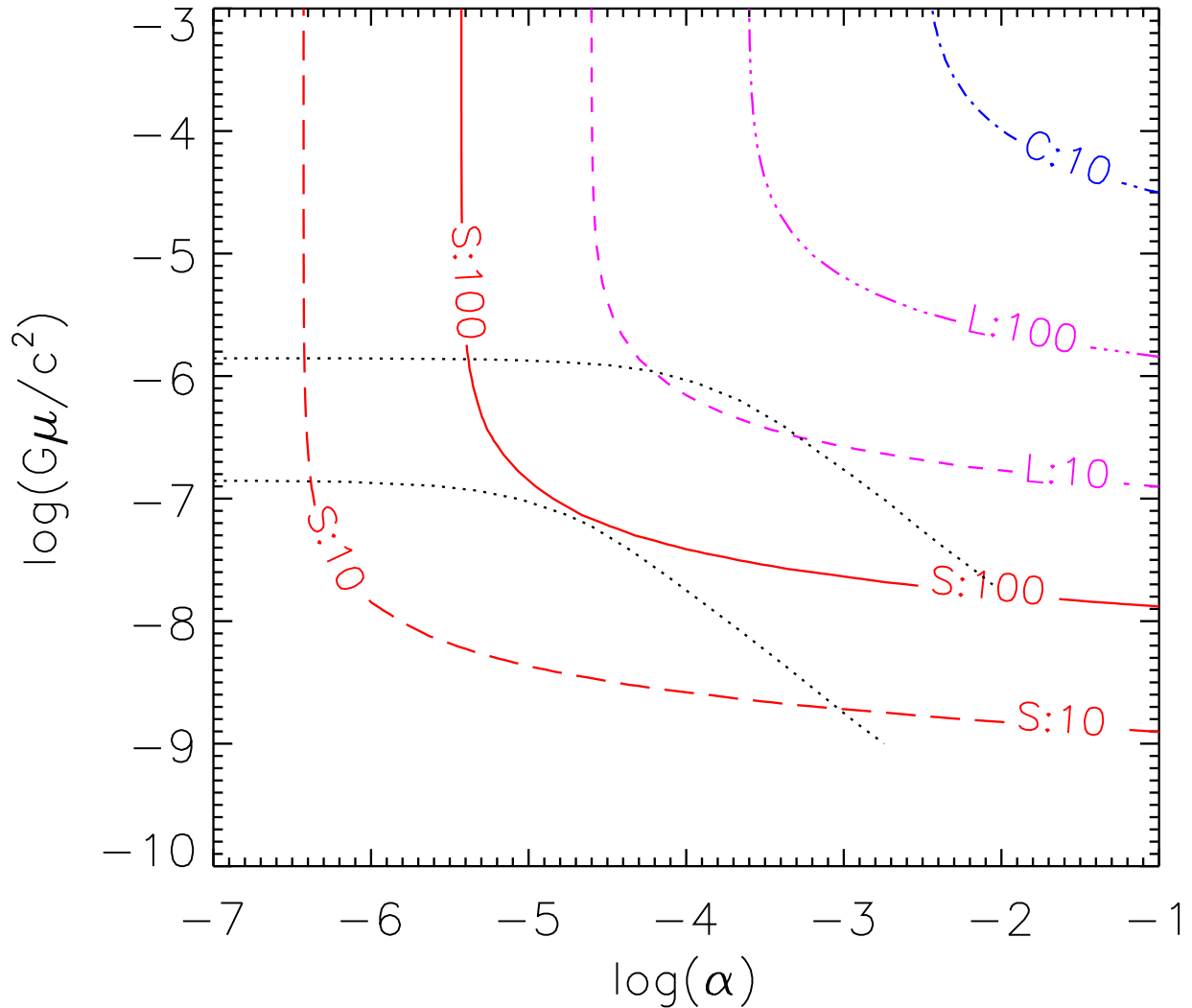


FIG. 3: Contours for 10 and 100 expected events using the one-scale loop spectrum model for CLASS/JVAS (C), LOFAR (L), and SKA (S), for a source population at redshift $z=1.2$. We also plot the pulsar timing constraint from [45] (black dotted lines). The upper dotted line is for $\Omega_g h^2 < 2 \times 10^8$ and the lower is for $\Omega_g h^2 < 2 \times 10^9$ – see [45] for a discussion of the uncertainty. In this plot, the x-axis is the one-scale model parameter α (see Section II B 2) and the y-axis is the dimensionless loop tension $G\mu/c^2$.

space.

However, a simple comparison between limits from the gravitational wave background and from loop lensing surveys can obscure the most important feature of a lensing survey, which is that it is a *direct search*. While constraints from pulsar timing rely on models

of the loop radiation and simulations of the behavior of loop networks, lensing relies only on the presence of a mass concentration, the effects of which are directly observed in the image distributions. Any model of a cosmic string population will make simple and testable predictions for gravitational lensing surveys.

IV. DISCUSSION

We have found that searching for lensed compact radio sources in future surveys can greatly improve constraints on cosmic string networks. Extending the excluded region of parameter space, or alternatively observing a cosmic string, will allow us to better understand physics beyond the Standard Model. We have shown that if no cosmic string loop lensing events are observed in upcoming radio surveys, much of the currently interesting parameter space can be ruled out, but further work is needed to determine what one could learn about the nature of cosmic strings if a lensing event were actually to be observed. For the sake of obtaining a constraint, it is sufficient to discuss the scenario in which all lensing events in a survey can be accounted for by the detection of a conventional lensing object (such as a galaxy or cluster) in follow-up observations, so there is no need to invoke cosmic strings. In all known strong gravitational lensing events to date, observations have identified the source of the lensing potential as a standard baryonic or dark-matter structure.

In this work, we have tried to make conservative assumptions in order to estimate the lensing signal, but including additional effects is only likely to improve our limits. For instance, the statistically complete sample of lenses in CLASS [36] includes only those systems with flux ratio less than 10:1, but future radio interferometers with higher dynamic range may be expected to easily improve on this ratio by at least an order of magnitude. This would significantly increase the effective lensing area for each loop to as much as an order of magnitude above the area within the Einstein radius.

In any survey, brighter events are more likely to be above the flux limit, and so lensing surveys will see a disproportionate number of high-magnification events. By not explicitly including the effect of this magnification bias in our estimate, we are underestimating the number of lensed sources.

The detailed properties of the cosmic strings under consideration will also likely enhance their prospects for detection. One such property is the reconnection probability P , which

is unity for ordinary cosmic strings [46], but can be significantly less than unity for cosmic strings originating from superstring models [22, 47]. Simulations indicate that for $P < 0.1$, the string number density increases as $\sim P^{-0.6}$ [48], which would proportionally increase the number of expected lensing events. In addition, there may be several distinct string populations present: for example, in brane inflation scenarios multiple types of cosmic strings, labeled by coprime integers (p, q) , would be produced. The total number of strings would be enhanced by the number of different populations present [49], enhancing the lensing signal by the same factor.

Further work on the statistical properties of loop lensing will help to sharpen our constraint. We expect that considering lensing by loops in more general configurations (including oscillations) will only slightly affect the total lensing cross section. However, understanding the effects of configuration may be important for determining the detailed properties of individual loops detected in lensing surveys.

Experiments such as LISA will revolutionize the observation of gravitational waves, in particular the stochastic background, to which cosmic strings are expected to contribute a distinctive signature [50]. In comparison with limits from millisecond pulsars, LISA is expected to push back the minimum detectable string threshold by ~ 7 orders of magnitude [44]. Although these tensions are inaccessible to the surveys we mention in this work, a lensing search is a complementary technique in that in addition to requiring fewer assumptions about the behavior of strings, it involves a local phenomenon rather than a spectral signature from a population.

We hope that our results will motivate the optimization of future surveys for events of this nature. The next generation of radio surveys have the potential to directly detect cosmic string loops, opening a new window into the physics of the early universe.

V. ACKNOWLEDGEMENTS

This work was supported in part by a NSF Graduate Research Fellowship (KJM). KJM would like to acknowledge useful discussions with George Efstathiou, Rob Fender, Tom Maccarone, David Spergel and Paul Steinhardt and the hospitality of the IoA and DAMTP (Cambridge University) during the time this work was carried out. LJK is supported by the Royal Society. She also thanks Antony Lewis, Guy Pooley and Elizabeth Waldram

for useful discussions. DHW thanks Mark Wyman for informative discussions, and the Perimeter Institute for its hospitality during the final stages of this work.

APPENDIX A: ONE-SCALE MODEL LOOP SPECTRUM

In this Appendix we describe the process by which the loop length distribution (6) and total mass in loops (7) are derived in the context of the one-scale model (OSM). The equations and parameter values we use are those of [4]. According to the OSM, the energy density in long strings scales like ℓ^{-2} where ℓ is the particle horizon, defined by

$$\ell(t) = a(t) \cdot \int_0^t \frac{dt'}{a(t')} = 3ct, \quad (\text{A1})$$

and the last equality holds during matter domination. Applying energy conservation then determines the rate at which the long string network sheds energy in the form of loops. The loops formed at time t are all taken to have an initial length $\alpha\ell(t)$, where α is a dimensionless constant. These assumptions imply that the absolute number N of loops created in a comoving cubical volume of size R on a side is given by

$$\frac{dN}{d\ell} = \frac{a(t)^3 R^3}{\ell^4} \cdot \frac{C}{\alpha} = \frac{C}{4\alpha} \frac{\ell_{H0}}{\ell^2} \quad (\text{A2})$$

where $C = 5.3$ during matter domination. To obtain the second equality, we have taken $a = 1$ at a fiducial time t_0 , and used $a(t) = (t/t_0)^{2/3} = (\ell/2\ell_{H0})^{2/3}$, where $\ell_{H0} = c/H(t)$ is the Hubble length at t_0 . We have further taken $R = \ell_{H0}$, so N is the number of loops in a comoving (cubical) horizon volume.

Once loops have formed, they begin to shrink as they lose energy by emitting gravitational radiation. The energy loss rate is

$$\frac{dE}{dt} = -\Gamma G\mu^2 c, \quad (\text{A3})$$

where $\Gamma \sim 50$ is taken from simulations. This means that the length of a loop that was “born” at time t_B is

$$L(t, t_B) = f_r \alpha \ell(t_B) - \frac{\Gamma G\mu}{c} (t - t_B), \quad (\text{A4})$$

where $f_r \sim 0.7$ is a factor accounting for the shrinking of the loop as its initial relativistic velocity is redshifted by Hubble expansion. During matter domination the time t_D at which

a loop “dies” (completely evaporates) is related to its time of birth by

$$t_D = \frac{t_B}{\beta}, \quad \beta = \left(1 + \frac{3f_r\alpha c^2}{\Gamma G\mu}\right)^{-1}. \quad (\text{A5})$$

This also means that a loop of length L , observed when the particle horizon is ℓ , was born when the particle horizon was a size ℓ_B given by

$$\ell_B = \beta \left(\ell + \frac{3c^2}{\Gamma G\mu}L\right). \quad (\text{A6})$$

In our universe, if $\beta > 5 \times 10^{-6}$, then all the loops created during radiation domination will have evaporated by the present day. We will assume this is so in the following.

Our first goal is to calculate the spectrum of loop lengths, evaluated at the fiducial time t_0 . We proceed by writing

$$L \frac{dN}{dL} \Big|_{t_0} = L \frac{dN}{d\ell_B} \frac{d\ell_B}{dL} \quad (\text{A7})$$

where ℓ_B is the particle horizon length when a loop currently of length L was created. The first derivative on the right hand side is given by (A2), and the second is obtained from (A6). Combining them, we find

$$L \frac{dN}{dL} \Big|_{t_0} = \frac{3}{16} \frac{C c^2}{\alpha \beta \Gamma G\mu} \frac{L/\ell_{H0}}{\left(1 + \frac{L}{2\Gamma G\mu\ell_{H0}/3c^2}\right)^2}, \quad (\text{A8})$$

which, once the values for f_r, Γ and C are substituted, becomes precisely equation (6).

To compute the density parameter in loops, we first calculate the total length in loops. This requires the integral identity

$$\int_0^{L_*} \frac{AL/B}{(1 + L/B)^2} dL = AB \left[\ln \left(1 + \frac{L_*}{B}\right) - \frac{L_*/B}{1 + L_*/B} \right], \quad (\text{A9})$$

which applies to our case with the choice,

$$A = \frac{C}{8\alpha\beta}, \quad B = \frac{2\Gamma G\mu\ell_{H0}}{3c^2}, \quad L_* = \alpha\ell = 2\alpha\ell_{H0}. \quad (\text{A10})$$

The upper cutoff is necessary because the largest possible loops are those being created right at t_0 . The integral formula gives

$$L_{loop}^{(tot)} = \ell_{H0} \cdot \frac{\Gamma C}{12y} \left(1 + \frac{3f_r}{\Gamma}y\right) \left[\ln \left(1 + \frac{3}{\Gamma}y\right) - \left(1 + \frac{\Gamma}{3y}\right)^{-1} \right] \quad (\text{A11})$$

where we have taken $y = \alpha/(G\mu/c^2)$. From the standard definition of the density parameter, we have

$$\Omega_{loop} = \frac{8\pi}{3} \frac{L_{loop}^{(tot)}}{\ell_{H0}} \left(\frac{G\mu}{c^2}\right). \quad (\text{A12})$$

Finally, substituting the values of f_r , Γ and C we obtain equation (7).

- [1] Kibble, T.W.B. 1976, J. Phys. A9, 1387
- [2] Hindmarsh, M.B. & Kibble, T.W.B. 1995, Rept. Prog. Phys. 58, 477
- [3] Vilenkin, A. & Shellard, E.P.S. 2000, Cosmic Strings and Other Topological Defects (Cambridge:CUP)
- [4] Caldwell, R.R. & Allen, B. 1992, PhysRevD, 45, 3447
- [5] Caldwell, R.R., Battye, R.A., & Shellard, E.P.S. 1996, PhysRevD, 54, 7146
- [6] Landriau, M. & Shellard, E.P.S. 2004, PhysRevD, 68, 023003
- [7] Pogosian, L., Wyman, M.C. & Wasserman, I. 2004, JCAP, 09, 008
- [8] Pogosian, L., Wyman, M.C. & Wasserman, I. 2006, astro-ph/0604141
- [9] Jeong, E. & Smoot, G.F. 2005, ApJ, 624, 21
- [10] Pogosian, L. et al. 2003, PhysRevD, 68, 023506
- [11] Pen, U-L, Seljak, U. & Turok, N. 1997, PhysRevLett, 79, 1611
- [12] Allen, B. et al. 1997, PhysRevLett, 79, 2624
- [13] Albrecht, A., Battye, R.A., & Robinson, J. 1999, PhysRevD, 59, 023508
- [14] Spergel, D.N. et al. 2006, astro-ph/0603449
- [15] Wyman, M., Pogosian, L. & Wasserman, I. 2006, PhysRevD, 72, 023513; Erratum-ibid. 2006, PhysRevD, 73, 089905
- [16] Sazhin, M.V. 2006, astro-ph/0611744
- [17] Shlaer, B. & Wyman, M. 2005, PhysRevD, 72, 123504
- [18] Seljak, U. & Slosar, A. 2006, PhysRevD, 74, 063523
- [19] Dvali, G. & Tye, S.-H.H. 1999, PhysLettB, 450, 72
- [20] Jones, N. et al. 2002, JHEP, 07, 051
- [21] Saswat Sarangi, S. & Tye, S.-H.H. 2002, PhysLettB, 536, 185
- [22] Jones, N.T., Stoica, H. & Tye, S.-H.H. 2003, PhysLettB, 563, 6
- [23] Witten, E. 1985, PhysLettB, 153, 243
- [24] Copeland, E.J., Myers, R.C. & Polchinski, J. 2004, JHEP, 06, 013
- [25] Polchinski, J. 2005, Int. J. Mod. Phys. A., 20, 3413
- [26] Huterer, D. & Vachaspati, T. 2003, PhysRevD, 68, 041301

- [27] Uzan, J.-P. & Bernardeau, F. 2000, *PhysRevD*, 63, 023004
- [28] de Laix, A.A. & Vachaspati, T. 1996, *PhysRevD*, 54, 4780
- [29] Hogan, C. & Narayan, R. 1984, *MNRAS*, 211, 575
- [30] Schneider, P., Ehlers, E. & Falco, E. 1992, *Gravitational Lenses* (Berlin/Heidelberg/New York:Springer-Verlag)
- [31] Vanchurin, V., Olum, K.D. & Vilenkin, A. 2006, *PhysRevD*, 74, 063527
- [32] Ringeval, C., Sakellariadou, M. & Bouchet, F. 2005, *astro-ph/0511646*
- [33] Marlow, D.R. et al. 2000, *AJ*, 119, 2629
- [34] Dobke, B.M. & King, L.J. 2006, *A&A*, 460, 647
- [35] Falco, E.E., Kochanek, C.S. & Munoz, J.A. 1998, *ApJ*, 494, 47
- [36] Browne, I.W.A. et al. 2003, *MNRAS*, 341, 13
- [37] Myers et al. 2003, *MNRAS*, 341, 1
- [38] King, L.J. et al. 1999, *MNRAS*, 307, 225
- [39] Vogt, C. (editor) 2006, “A Science Case for an Extended LOFAR,” ASTRON (Dwingeloo, The Netherlands)
- [40] Wucknitz, O. et al. 2006, in “A Science Case for an extended LOFAR,” ASTRON (Dwingeloo, The Netherlands)
- [41] Cohen, A. 2005, in *URSI Commission J Meeting* (Boulder:University of Colorado), <http://astro.uchicago.edu/ursi-comm-J/ursi2005/>
- [42] Koopmans, L., Browne, I.W.A. & Jackson, N. 2004, *New Astronomy Reviews*, 48, 1085
- [43] Carr, B.J. 1975, *ApJ*, 201, 1
- [44] DePies, M.R. & Hogan, C.J. 2007, *astro-ph/0702335*
- [45] Battye, R.A., Garbrecht, B. & Moss, A. 2006, *JCAP*, 0609, 007
- [46] Shellard, E.P.S. 1987, *Nucl. Phys. B*, 283, 624
- [47] Jackson, M.G., Jones, N.T. & Polchinski, J. 2004, *hep-th/0405229*
- [48] Avgoustidis, A. & Shellard, E.P.S. 2006, *PhysRevD*, 73, 041301
- [49] Tye, S.-H.H., Wasserman, I. & Wyman, M. 2005, *PhysRevD*, 71, 103508; Erratum-ibid. 2005, *PhysRevD*, 71, 129906
- [50] Hogan, C.J. 2006, *astro-ph/0608567*